Journal of Physics: Conference Series

PAPER • **OPEN ACCESS**

Characterization of Light Diffraction by a Digital Micromirror Device

To cite this article: C Pereira *et al* 2022 *J. Phys.: Conf. Ser.* **2407** 012048

Characterization of Light Diffraction by a Digital Micromirror Device

C Pereira[1,2,3], M Abreu[1,2], A Cabral[1,2] and J M Rebordão[1,2]

[1] Instituto de Astrofísica e Ciências do Espaço, Universidade de Lisboa, Campo Grande, 1749-016 Lisboa, Portugal

[2] Faculdade de Ciências da Universidade de Lisboa, Departamento de Física, Campo Grande, 1749-016 Lisboa, Portugal

[3] Email: cppereira@fc.ul.pt

Abstract. A Digital Micromirror Device (DMD) is a technology developed by Texas Instruments, that consists in a two-dimensional array of micromirrors, which can be individually tilted between two positions. It has been used as a digital video and image processing solution, commonly found in Digital Light Processing (DLP) video projectors. Over the years, DMDs have become popular in different fields: industrial, automotive, medical, government and home user solutions. In the astronomy field, it has been also considered in on-ground space instrumentation and it has been proposed for the development of some astrophysical space instruments. In order to evaluate the actual impact of such device in the instrument optical design, it is important to know how the light behaves when it interacts with a DMD, namely in what regards to the diffraction process when a light beam is reflected by a periodic array of micromirrors. In this study we describe how we simulate the diffraction patterns produced by a periodic array of micromirrors, for coherent and incoherent sources of light. The results from simulations are verified against laboratory experiments, described also in this study.

Keywords: instrumentation, diffraction, digital micromirror device.

1. Introduction

A Digital Micromirror Device (DMD) is a technology developed by Texas Instruments, in 1987, that consists in a two-dimensional array of micromirrors [1] that can be individually tilted between two positions, typically ± 12° in reference to the normal of the DMD chip [2]. It has been used as a digital video and image processing solution, commonly found in Digital Light Processing (DLP) video projectors [3].

In a video projector, each micromirror represents one pixel in the projected image. If a micromirror is in the ON state (typically +12°), the reflected light is sent through a set of lenses contributing to the projected image, while in the OFF state (typically -12°), the reflected light is sent in the direction of a heatsink, to be dissipated. With this system, it is possible to control the brightness of each pixel, switching the micromirror to the ON state (white pixel), to the OFF state (dark pixel), or toggling it at high frequencies between the two positions (grayscale) [2-3].

Over the years, DMDs have become popular in different areas: industrial sector (control panels, human-machine interfaces, 3D vision system, holography, lithography), automotive sector (displays, center consoles, intelligent lighting systems), medical sector (medical spectroscopy, 3D printing, 3D vision), government sector (education, cinema, mobile projection) or even in the home user sector (video games systems, mobile phones, tablets, computers, home automation) [4]. With such versatility, it is also considered for space instrumentation [5]. One of the most popular cases is the integration of DMDs in spectrographs, in order to create multiple slits, to get the spectrum of multiple astronomical objects at the same time. Some instruments like IRMOS [6], RITMOS [7] and BATMAN [8] were designed based on this technology. DMDs were also proposed to the development of some space mission instruments, for example the JWST [5] and EUCLID [9], however, this technology is not yet available with space certification. DMDs have also become popular in wavefront shaping techniques. Liquid crystal spatial light modulators (LCSLM) are traditionally used when it is required to modulate a wavefront, but their low refresh rates are a major limitation. DMDs can be a potential solution for LCSLM speed limitation, as they enable much faster modulation speeds (kHz-order) [10].

With a good representation in different fields, DMDs are an important technology for the scientific research community. To successfully make use of this technology, it is important to know how the light behaves when it is reflected by a DMD. When a beam of light is reflected by this periodic array of micromirrors, diffraction patterns will be produced according with different conditions, starting in the wavelength range, up to the state or the angle of each micromirrors.

This study presents an exploratory work on the technical feasibility of using DMDs for optical applications, focusing on the diffraction patterns produced by an array of micromirrors. This is not only important for space technologies, but it has relevance to every technology that uses adaptative optics. To cover a wide range of potential applications, it is considered two types of light sources (coherent and incoherent light) and a successful DMD on the market, commonly used in some evaluation boards (TI DLP7000 1024x768 XGA) [11]. The simulations are verified against laboratory experiments.

2. Simulation of Diffraction Patterns

The approach chosen to calculate the diffraction pattern produced by a DMD starts by studying first the simplest cases, as for example, the diffraction pattern produced by a single square aperture, going further in the degree of complexity until the final structure. This study takes into account the Fraunhofer approximation methodology, valid when the source of light and the target screen are placed at infinite distances from the obstacle/aperture (far field) [12]. A plane wavefront reaches and emerges from the obstacle/aperture. This can be performed in the laboratory using two convex lenses, one to collimate the beam of light from a point source and another to focus the diffracted light onto the target screen (Fourier plane).

2.1. Single Square Aperture

When a beam of light reaches an obstacle with a square aperture and the size of the square aperture is comparable to the wavelength of the incident wave, spherical wavefronts are emitted from different sections of the aperture. The interference of those spherical wave fronts creates a diffraction pattern on the screen target.

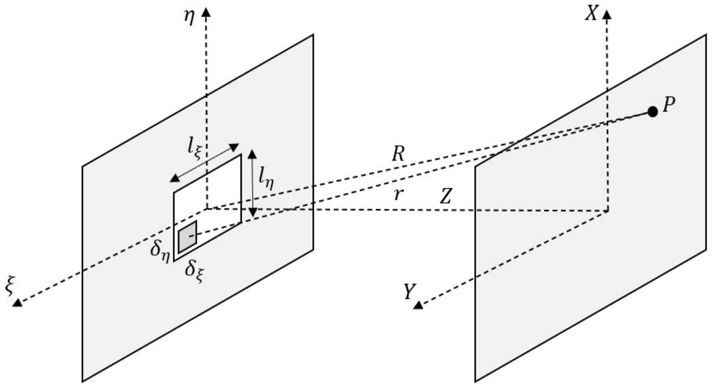

Figure 1. Diagram taking into consideration to calculate the diffraction pattern of a square aperture. The diffraction aperture is placed at the (ξ,η) plane, with the origin of this coordinated system at the center of the square aperture and the screen target is placed at the (X,Y) plane. The Z axis is shared by both coordinate systems. The planes are parallel to each other, at a normal distance z. $\delta\xi$ and $\delta\eta$ represent an arbitrary small area of the square aperture, where a wavefront is emitted and contributes to the diffraction pattern at an arbitrary point p, at a distance r from the center of the small area $(\delta\xi,\ \delta\eta)$ and at a distance R from origin of the (ξ,η) coordinate system.

The following calculations follow the derivation of the Fraunhofer diffraction approximation indicated in the Goodman Fourier Optics [12] textbook. The Fraunhofer far field equation can be seen as the Fourier transform of the aperture distribution function $\mathrm{U}(\xi,\eta)$, evaluated at spatial frequencies $f_x=\frac{x}{\lambda z}$ and $f_y=\frac{y}{\lambda z}$:

$$\mathrm{U}(x,y)=\frac{\mathrm{e}^{\mathrm{j}kz}\mathrm{e}^{\mathrm{j}\frac{k}{2z}(x^2+y^2)}}{\mathrm{j}\lambda z}\int_{-\infty}^{\infty}\int \mathrm{U}(\xi,\eta)\,\mathrm{e}^{\mathrm{j}\frac{2\pi}{\lambda z}(x\xi+y\eta)}\,d\xi d\eta \tag{2.1.1}$$

$$\mathrm{U}(x,y)=\frac{\mathrm{e}^{\mathrm{j}kz}\mathrm{e}^{\mathrm{j}\frac{k}{2z}(x^2+y^2)}}{\mathrm{j}\lambda z}\mathfrak{F}[\mathrm{U}(\xi,\eta)]\big|_{f_x=\frac{x}{\lambda z},\ f_y=\frac{y}{\lambda z}} \tag{2.1.2}$$

The amplitude transmittance of a single square aperture is given by the product of two rectangular functions, where l_ξ, l_η are the aperture widths in ξ,η directions:

$$\tau_{\mathrm{A}}(\xi,\eta)=\mathrm{rect}\left(\frac{\xi}{l_\xi}\right)\mathrm{rect}\left(\frac{\eta}{l_\eta}\right) \tag{2.1.3}$$

The following equation shows the Fourier transform of equation (2.1.3), where A is the area of the square aperture:

$$\mathfrak{F}[\tau_{\mathrm{A}}(\xi,\eta)]=A\,\mathrm{sinc}\big(l_\xi\,f_x\big)\,\mathrm{sinc}(l_\eta\,f_y) \tag{2.1.4}$$

From equations (2.1.2) and (2.1.4):

$$\mathrm{U}(x,y) = \frac{\mathrm{e}^{\mathrm{j}kz}\mathrm{e}^{\mathrm{j}\frac{k}{2z}(x^2+y^2)}}{\mathrm{j}\lambda z} A \,\mathrm{sinc}\left(\frac{l_\xi x}{\lambda z}\right)\mathrm{sinc}\left(\frac{l_\eta y}{\lambda z}\right) \tag{2.1.5}$$

The intensity is given by:

$$\mathrm{I}(x,\mathrm{y}) = \frac{A^2}{\lambda^2 z^2}\mathrm{sinc}^2\left(\frac{l_\xi x}{\lambda z}\right)\mathrm{sinc}^2\left(\frac{l_\eta y}{\lambda z}\right) \tag{2.1.6}$$

The simulation of the diffraction pattern given by a square aperture is shown in figures 2 and 3, for coherent and incoherent light sources, respectively. For an incoherent light source, a diffraction pattern is calculated for each wavelength and the resulting irradiances are integrated. Depending on the type of the light source, each wavelength contributes with a different weight to the final result.

The diffraction pattern shows a central square lobe with successive horizontal and vertical fringes. The size of the central lobe is related with the size of the square aperture, the distance between the aperture and the target screen and with the wavelength of the incident light. The separation between fringes is inversely proportional to the size of the square aperture. Figure 3 is the simulation of the diffraction pattern for a black body source at 10 000 K. Such light source has a wide range of wavelengths, not in phase to each other and whose photons oscillate at different frequencies. In the image, for the same order, it is possible to observe that each wavelength is shifted with respect to each other, as the diffraction angle depends on the wavelength and longer wavelengths produced larger diffraction angles.

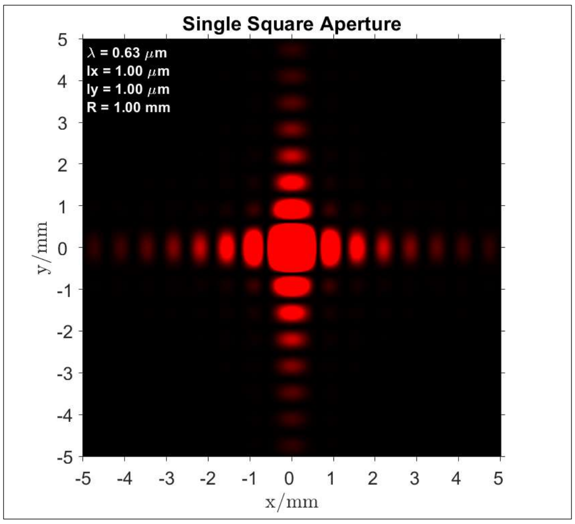

Figure 2. Diffraction pattern simulation of a square aperture, for a coherent light source, with a wavelength of 632 nm, passing through a 1 µm square aperture, projected onto a target at 1 mm distance with 10x10 mm area.

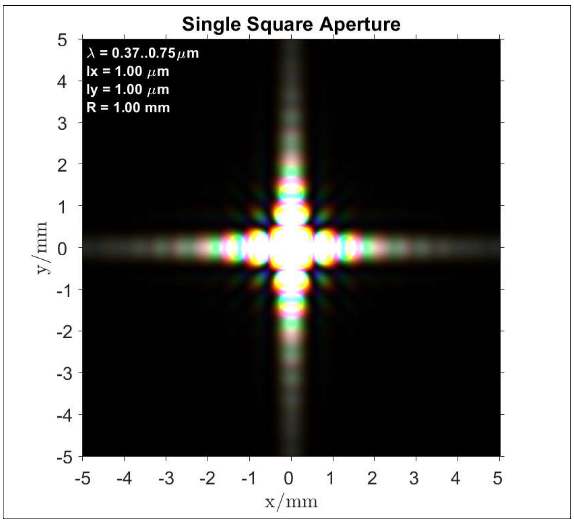

Figure 3. Diffraction pattern simulation of a square aperture, for a black body at a temperature of 10 000 K, with a wavelength range from 375 nm to 750 nm, passing through a 1 µm square aperture, projected onto a target at 1 mm distance with 10x10 mm area.

2.2. Two-dimensional Array of Square Apertures

When a beam of light reaches an obstacle with an array of square apertures, multiple spherical wavefronts are emitted from each aperture, interfering with each other and creating a diffraction pattern.

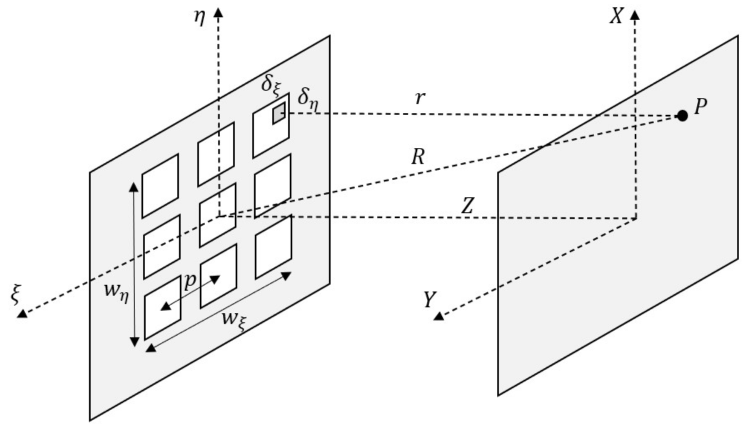

Figure 4. Diagram taking into consideration to calculate the diffraction pattern of a two-dimensional array of square apertures. The aperture array is placed at the (ξ, η) plane and the screen target is placed at the (X, Y) plane. The Z axis is shared by both coordinate systems. The planes are parallel to each other, at a normal distance z. $\delta\xi$ and $\delta\eta$ represent an arbitrary small area of one square aperture, where a wavefront is emitted and contributes to the diffraction pattern at an arbitrary point p, at a distance r from the center of the small area $(\delta\xi,\ \delta\eta)$ and at a distance R from origin of the (ξ, η) coordinate system.

The amplitude transmittance of a two-dimensional array of square apertures is given by the product of two rectangular functions convolved with a comb function (convolution is denoted by the symbol ⊗), multiplied by the product of two another rectangular functions to delimitate the aperture array area, where l_ξ, l_η are the aperture widths in ξ, η directions, w_ξ, w_η are the dimensions of the aperture array in ξ, η directions and p is the pitch between apertures:

$$\tau_\mathrm{A}(\xi, \eta) = \left[\mathrm{rect}\left(\frac{\xi}{l_\xi}\right)\mathrm{rect}\left(\frac{\eta}{l_\eta}\right) \otimes \mathrm{comb}\left(\frac{\xi}{p}\right)\mathrm{comb}\left(\frac{\eta}{p}\right)\right]\mathrm{rect}\left(\frac{\xi}{w_\xi}\right)\mathrm{rect}\left(\frac{\eta}{w_\eta}\right) \tag{2.2.1}$$

Equation (2.2.1) can be expressed into a series of sums to simplify the comb functions:

$$\tau_\mathrm{A}(\xi, \eta) = \sum_{i\,j} \mathrm{rect}\left(\frac{\xi - \xi_{ij}}{l_\xi}, \frac{\eta - \eta_{ij}}{l_\eta}\right) \tag{2.2.2}$$

The Fourier shift theorem can be used to do the Fourier transform of equation (2.2.2):

$$\mathfrak{F}[\mathrm{g}(x, y)] = \mathrm{G}(f_x, f_y) \tag{2.2.3}$$

$$\mathfrak{F}[\mathrm{g}(x - a, y - b)] = \mathrm{G}(f_x, f_y)\, \mathrm{e}^{-2\pi \mathrm{j}(f_x\, a + f_y\, b)} \tag{2.2.4}$$

The following equation shows the Fourier transform of equation (2.2.2), where A is the area of the square aperture:

$$\mathfrak{F}[\tau_A(\xi,\eta)] = A\,\mathrm{sinc}\big(l_\xi\, f_x\big)\,\mathrm{sinc}\big(l_\eta\, f_y\big)\sum_{i,j} \mathrm{e}^{-2\pi\mathrm{j}(\xi_{ij}\, f_x + \eta_{ij}\, f_y)} \tag{2.2.5}$$

From equations (2.1.2) and (2.2.5):

$$\mathrm{U}(x,y) = \frac{\mathrm{e}^{\mathrm{j}kz}\mathrm{e}^{\mathrm{j}\frac{k}{2z}(x^2+y^2)}}{\mathrm{j}\lambda z} A\,\mathrm{sinc}\left(\frac{l_\xi x}{\lambda z}\right)\mathrm{sinc}\left(\frac{l_\eta y}{\lambda z}\right)\sum_{i,j} \mathrm{e}^{-2\pi\mathrm{j}\left(\frac{x\,\xi_{ij}}{\lambda z}+\frac{y\,\eta_{ij}}{\lambda z}\right)} \tag{2.2.6}$$

The intensity is given by:

$$\mathrm{I}(x,\mathrm{y}) = \frac{A^2}{\lambda^2 z^2}\mathrm{sinc}^2\left(\frac{l_\xi x}{\lambda z}\right)\mathrm{sinc}^2\left(\frac{l_\eta y}{\lambda z}\right)\left[\sum_{i,j} \mathrm{e}^{-2\pi\mathrm{j}\left(\frac{x\,\xi_{ij}}{\lambda z}+\frac{y\,\eta_{ij}}{\lambda z}\right)}\right]^2 \tag{2.2.7}$$

The simulation of the diffraction pattern given by a two-dimensional array of square apertures is shown in figures 5 and 6, for coherent and incoherent light sources, respectively. For an incoherent light source, a diffraction pattern is calculated for each wavelength and the resulting irradiances are integrated. Depending on the type of the light source, each wavelength contributes with a different weight to the final result.

In a two-dimensional array of square apertures, the light coming from each aperture interfere with each other, creating multiple orders. For this case, where all apertures have the same size, the intensity of those orders depends on the diffraction envelop calculated from the width of a single aperture. The intensity of central orders is higher than in the periphery. The width of a single aperture and the separation between apertures, have a major role in the final geometry of the diffraction pattern. A greater number of apertures contributes to narrower and higher intensity peaks. In figure 6 is the simulation of the diffraction pattern for a black body source at 10 000 K. Such light source has a wide range of wavelengths, not in phase to each other and whose photons oscillate at different frequencies. In the image, for the same order, it is possible to observe that each wavelength is shifted to each other, as the diffraction angle depends on the wavelength and longer wavelengths produced larger diffraction angles.

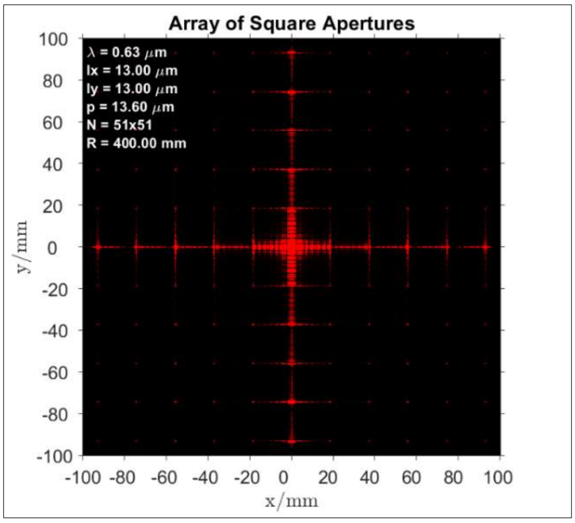

Figure 5. Diffraction pattern simulation of a two-dimensional array of square apertures, for a coherent light source, with a wavelength of 632 nm, passing through an array of 51x51 square apertures, with 13 µm in size and with a spatial frequency of 13.6 µm, projected onto a target at 400 mm distance with 200x200 mm area.

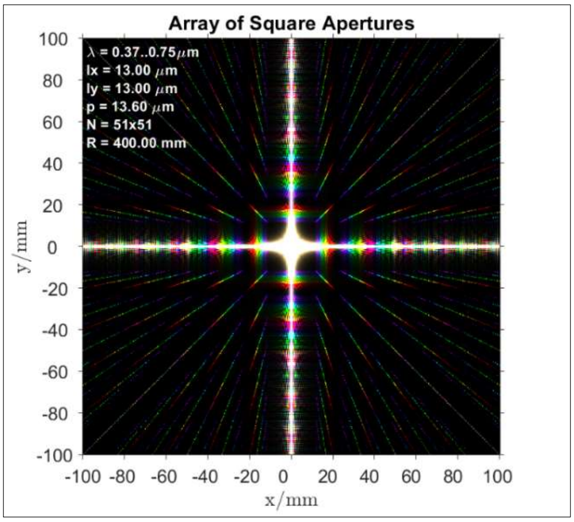

Figure 6. Diffraction pattern simulation of a two-dimensional array of square apertures, for a black body at a temperature of 10 000 K, with a wavelength range from 375 nm to 750 nm, passing through an array of 51x51 square apertures, with 13 µm in size and with a spatial frequency of 13.6 µm, projected onto a target at 400 mm distance with 200x200 mm area.

2.3. Two-dimensional Array of Tilted Micromirrors

To simulate the diffraction pattern created by a DMD, the apertures are now replaced by micromirrors, rotated θ degrees along their diagonal. Figure 8 represents a single micromirror (in yellow), rotated in reference to the plane contained in the (ξ, η) coordinate system (in grey). The rotation orientation is indicated in the figure.

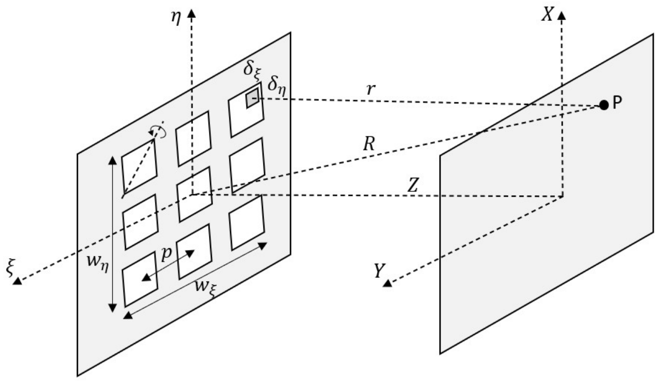

Figure 7. Diagram taking into consideration to calculate the diffraction pattern of a two-dimensional array of rotated micromirrors. The aperture array is placed at the (ξ, η) plane and the screen target is placed at the (X, Y) plane. The Z axis is shared by both coordinate systems. The planes are parallel to each other, at a normal distance z. $\delta\xi$ and $\delta\eta$ represent an arbitrary small area of one square aperture, where a wavefront is emitted and contributes to the diffraction pattern at an arbitrary point p, at a distance r from the center of the small area ($\delta\xi$, $\delta\eta$) and at a distance R from origin of the (ξ, η) coordinate system.

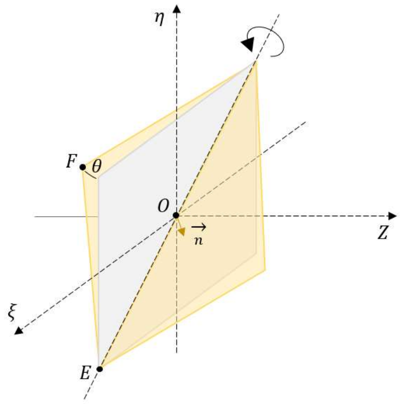

Figure 8. Diagram of a single rotated micromirror (in yellow). Represented in gray is the reference plane contained in the (ξ, η) coordinate system, perpendicular to the Z axis. In yellow is a plane rotated θ degrees along the diagonal of the reference plane. n represents the normal vector of the rotated plane.

The orientation of each micromirror can be expressed in the form of $Z(\xi, \eta) = a\xi + b\eta$ (from the general form of the equation of a plane), where a and b coefficients are related with the components of a normal vector to the surface plane of the micromirror. The normal vector depends on the rotation axis of the micromirror. It is assumed the center of each micromirror is located at $Z = 0$. It is possible to find the components of a vector normal to a plane, with two other vectors contained in the same plane. The cross product of two independent vectors is an orthogonal vector, normal to the plane that contains them. For this case it is used the vectors OE and OF. As the lengths l_ξ and l_η are the same for each micromirror, to simplify calculations, it is assumed $l_\xi = l_\eta = l$:

$$\underset{OE}{\rightarrow} = \left(\frac{l}{2}; -\frac{l}{2}; 0\right) \qquad \underset{OF}{\rightarrow} = \left(\frac{l}{2}\cos\theta ; \frac{l}{2}\cos\theta ; -\frac{l}{\sqrt{2}}\sin\theta\right) \tag{2.3.1}$$

$$\underset{n}{\rightarrow} = \underset{OE}{\rightarrow} \times \underset{OF}{\rightarrow} = \left(\frac{l^2}{2\sqrt{2}}\sin\theta ; -\frac{l^2}{2\sqrt{2}}\sin\theta \ ; \frac{l^2}{2}\cos\theta\right) \tag{2.3.2}$$

The amplitude transmittance of a two-dimensional array of tilted micromirrors is given by the product of two rectangular functions convolved with a comb function, multiplied by the product of two another rectangular functions to delimitate the aperture array area, where l is the size of the micromirror equal for both ξ, η directions, w_ξ, w_η are the dimensions of the aperture array in ξ, η directions and p is the pitch between apertures. For this case, associated with the first two rectangular functions, are the components ξ, η from the normal vector to the surface plane of the micromirror, expressed as $2jk(a\xi + b\eta)$. The factor $2jk$ accounts for a phase delay of incoming and outgoing light:

$$\tau_A(\xi,\eta) = \left\{\left[\mathrm{rect}\left(\frac{\xi}{l}\right)\mathrm{rect}\left(\frac{\eta}{l}\right)\mathrm{e}^{2jk\left(\frac{l^2}{2\sqrt{2}}\sin\theta\,\xi - \frac{l^2}{2\sqrt{2}}\sin\theta\,\eta\right)}\right]\otimes \mathrm{comb}\left(\frac{\xi}{p}\right)\mathrm{comb}\left(\frac{\eta}{p}\right)\right\} \times \mathrm{rect}\left(\frac{\xi}{w_\xi}\right)\mathrm{rect}\left(\frac{\eta}{w_\eta}\right) \tag{2.3.3}$$

Equation (2.3.3) can be expressed into a series of sums to simplify the comb functions:

$$\tau_A(\xi,\eta) = \sum_{i\,j}\mathrm{rect}\left(\frac{\xi-\xi_{ij}}{l},\frac{\eta-\eta_{ij}}{l}\right)\mathrm{e}^{2jk\left(\frac{l^2}{2\sqrt{2}}\sin\theta\,\xi - \frac{l^2}{2\sqrt{2}}\sin\theta\,\eta\right)} \tag{2.3.4}$$

To perform the Fourier transform of equation (2.3.4), it can be splitted in two parts and the results are then convoluted:

$$\mathfrak{F}\left[\sum_{i\,j}\mathrm{rect}\left(\frac{\xi-\xi_{ij}}{l},\frac{\eta-\eta_{ij}}{l}\right)\right] = A\,\mathrm{sinc}(l\,f_x)\,\mathrm{sinc}(l\,f_y)\sum_{i,j}\mathrm{e}^{-2\pi\mathrm{j}(\xi_{ij}\,f_x + \eta_{ij}\,f_y)} \tag{2.3.5}$$

$$\begin{aligned}\mathfrak{F}\left[\mathrm{e}^{2jk\left(\frac{l^2}{2\sqrt{2}}\sin\theta\,\xi - \frac{l^2}{2\sqrt{2}}\sin\theta\,\eta\right)}\right] &= \int_{-\infty}^{\infty}\mathrm{g}(\xi,\eta)\,\mathrm{e}^{-\mathrm{j}(f_x\xi+f_y\eta)}\,\mathrm{d}\xi\mathrm{d}\eta \\ &= \int_{-\infty}^{\infty}\mathrm{e}^{2jk\left(\frac{l^2}{2\sqrt{2}}\sin\quad\xi - \frac{l^2}{2\sqrt{2}}\sin\theta\,\eta\right)}\,\mathrm{e}^{-\mathrm{j}(f_x\xi+f_y\eta)}\,\mathrm{d}\xi\mathrm{d}\eta = \\ &= \delta\left(\frac{l^2}{\sqrt{2}}\sin\theta\,k - f_x;\ -\frac{l^2}{\sqrt{2}}\sin\theta\,k + f_y\right)\end{aligned} \tag{2.3.6}$$

$$\begin{aligned}\mathfrak{F}\{\tau_A(\xi,\eta)\} &= \mathfrak{F}\left[\sum_{i\,j}\mathrm{rect}\left(\frac{\xi-\xi_{ij}}{l},\frac{\eta-\eta_{ij}}{l}\right)\right]\otimes\mathfrak{F}\left[\mathrm{e}^{2jk\left(\frac{l^2}{2\sqrt{2}}\sin\theta\,\xi - \frac{l^2}{2\sqrt{2}}\sin\theta\,\eta\right)}\right] = \\ &= A\,\mathrm{sinc}[l\,(f_x - t_0)]\ \mathrm{sinc}[l\,(f_y + t_0)]\sum_{i,j}\mathrm{e}^{-2\pi\mathrm{j}[\xi_{ij}\,(f_x-t_0)+\,\eta_{ij}\,(f_y+t_0)]}\end{aligned} \tag{2.3.7}$$

In equation (2.3.7), the mathematical result $\left(\frac{l^2}{\sqrt{2}}\sin\theta\,k\right)$ is defined as t_0. From equations (2.1.2) and (2.3.7):

$$\mathrm{U}(x,y) = \frac{\mathrm{e}^{\mathrm{j}kz}\mathrm{e}^{\mathrm{j}\frac{k}{2z}(x^2+y^2)}}{\mathrm{j}\lambda z}A\,\mathrm{sinc}\left[l\,\left(\frac{x}{\lambda z} - t_0\right)\right]\,\mathrm{sinc}\left[l\,\left(\frac{y}{\lambda z} + t_0\right)\right]\sum_{i,j}\mathrm{e}^{-2\pi\mathrm{j}\left[\xi_{ij}\left(\frac{x}{\lambda z}-t_0\right)+\,\eta_{ij}\left(\frac{y}{\lambda z}+t_0\right)\right]} \tag{2.3.8}$$

The intensity is given by:

$$\mathrm{I}(x,\mathrm{y}) = \frac{A^2}{\lambda^2 z^2}\mathrm{sinc}^2\left[l\,\left(\frac{x}{\lambda z} - t_0\right)\right]\,\mathrm{sinc}^2\left[l\,\left(\frac{y}{\lambda z} + t_0\right)\right]\left\{\sum_{i,j}\mathrm{e}^{-2\pi\mathrm{j}\left[\xi_{ij}\left(\frac{x}{\lambda z}-t_0\right)+\,\eta_{ij}\left(\frac{y}{\lambda z}+t_0\right)\right]}\right\}^2 \tag{2.3.9}$$

The simulation of the diffraction pattern given by a two-dimensional array of tilted micromirrors is shown in figures 9 and 10, for coherent and incoherent light sources, respectively. For an incoherent light source, a diffraction pattern is calculated for each wavelength and the resulting irradiances are integrated. Depending on the type of the light source, each wavelength contributes with a different weight to the final result. Note that these simulations are still under development, which is why they look different from the previous ones.

The diffraction pattern changes according with the typology of the light source. For a coherent light source, the structure of the diffraction pattern is well defined, where the orders are mostly distributed in a dotted pattern (figure 9). For an incoherent light source, the structure of the diffraction pattern is distributed in a striped pattern (figure 10), as each wavelength is shifted to each other, due to changes in diffraction angles according with the wavelength. Since it is used a discrete vector of wavelengths, the stripes visualized in the simulations are not continuous.

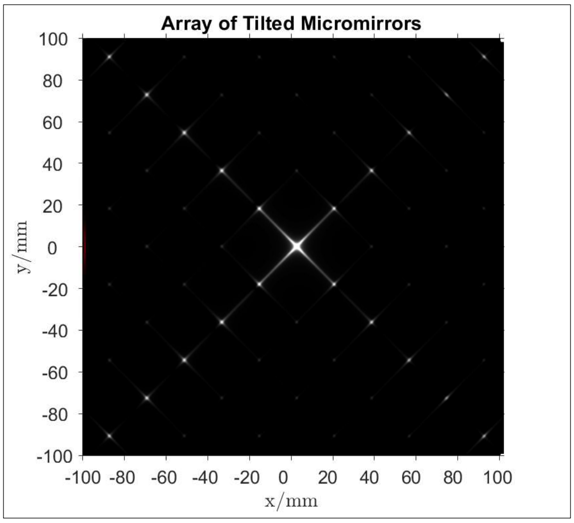

Figure 9. Diffraction pattern simulation of a two-dimensional array of tilted micromirrors, for a coherent light source, with a wavelength of 632 nm, falling in an array of 51x51 micromirrors rotated 12°, with 13 µm in size and with a spatial frequency of 13.6 µm, projected onto a target at 400 mm distance with 200x200 mm area.

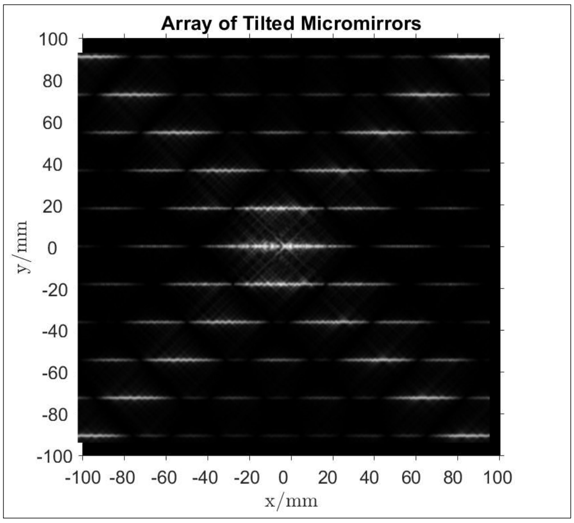

Figure 10. Diffraction pattern simulation of a two- dimensional array of tilted micromirrors, for a black body at a temperature of 10 000 K, with a wavelength range from 375 nm to 750 nm, falling in an array of 51x51 micromirrors rotated 12°, with 13 µm in size and with a spatial frequency of 13.6 µm, projected onto a target at 400 mm distance with 200x200 mm area.

3. Experimental Validation

To validate the calculations and simulations presented above, it is required to develop an experimental setup to observe the diffraction patterns resulting from each case: a single square aperture, a two-dimensional array of apertures and a two-dimensional array of tilted micromirrors.

3.1. Experimental Setup

The basic experimental setup to observe the diffraction patterns consists in two types of light sources, a coherent and an incoherent light source, collimating lens, to collimate the light beam coming from the light source through an optical fiber, a DMD, where the collimated light beam will be reflected/modulated, focusing lens, to collect the diffracted light, target screen, to visualize the diffraction pattern focused by the lens and a digital camera, to acquire scientific images. More secondary components are needed, as for example, a micrometer drive, to correctly adjust the position of collimating lens, a square aperture, to create a square light beam as used in the simulations, a cage mount, to assembly different optical elements, breadboard tables, electric connections, etc. It is also used a computer with a Labview interface specifically programmed to control the DMD board.

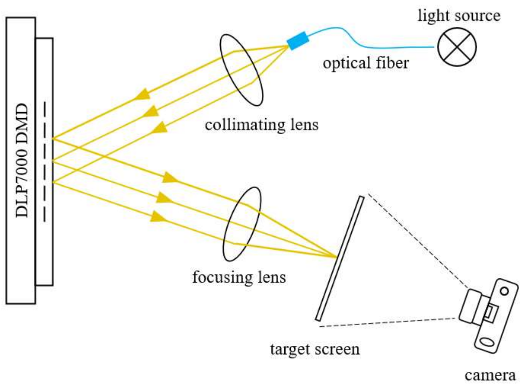

Figure 11. Diagram with the basic setup needed to perform the experimental validation of diffraction patterns. The key component is the DMD, configurable to obtain a two-dimensional array of square apertures and a two-dimensional array of tilted micromirrors.

The coherent light source chosen to perform the experimental validation is a Melles Griot Helium-Neon Laser, 30 mW, 632.8 nm; The incoherent source is a Thorlabs OSL1-EC Fiber Light Source, 150 W, 3200 K; The DMD chosen is a DLP D1100 EVM evaluation board with a DLP7000 DMD; The camera chosen to acquire scientific images is a Canon EOS 600D, 22.3 x 14.9 mm sensor size, 4.30 μm pixel size.

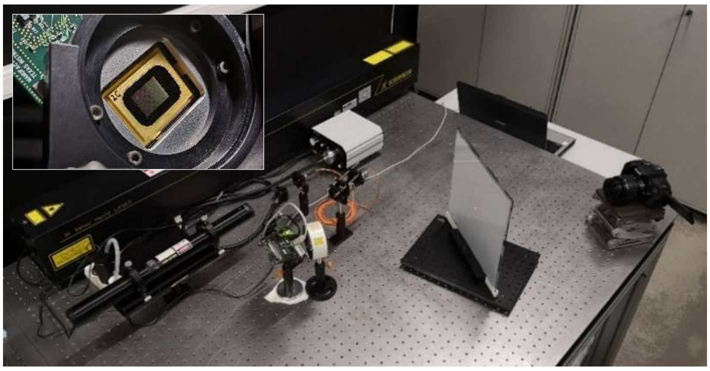

Figure 12. Laboratory setup to perform experimental validation of simulations.

The DMD can be controlled to obtain a two-dimensional array of square apertures or a two-dimensional array of tilted micromirrors. For the array of square apertures, the DMD needed to be commanded to place the micromirror in the FLAT state. Take into account that an array of micromirrors in the FLAT state acts as an array of apertures, resulting in the same diffraction pattern. When the micromirrors are in the FLAT state, they are not perfectly horizontal to each other [13], but rather slightly tilted to one side or the other, as represented on the top left image in figure 13. For the array of tilted micromirrors, the DMD needed to be commanded to place the micromirror in the ON or OFF state, where the micromirrors are tilted +12° or -12° in reference to the normal of the DMD chip, as represented on the right side of figure 13.

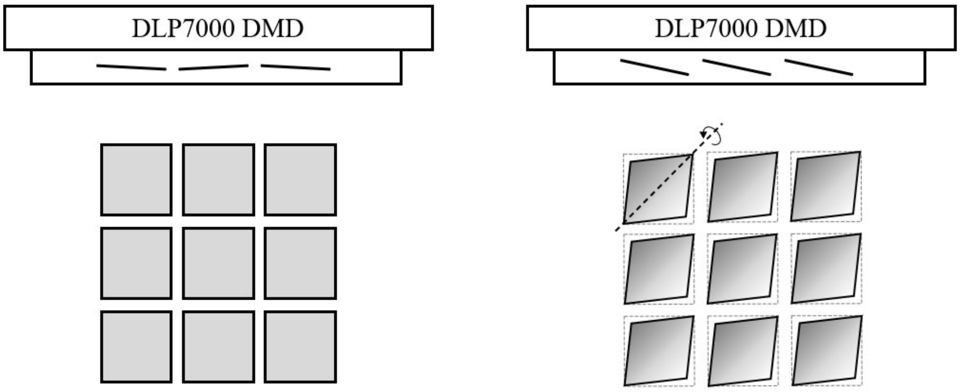

Figure 13. DMD micromirrors states. On the left side is the representation of micromirrors when they are in the FLAT state. When in this state, the micromirrors are not perfectly horizontal to each other, but rather slightly tilted to one side or the other. On the right side is the representation of micromirrors when they are in the ON state, tilted +12° in reference to the normal of the DMD chip. Switching between these states, it is possible to obtain a two-dimensional array of square apertures or a two-dimensional array of tilted micromirrors.

3.2. Experimental Results

Figures 14 (simulation) and 15 (experimental image) shows the diffraction patterns observable with a coherent light source, with a wavelength of 632 nm, for a two-dimensional array of square apertures. Figures 16 (simulation) and 17 (experimental image) shows the diffraction patterns observable with an incoherent light source, with a black body equivalent temperature of 3200 K, for a two-dimensional array of square apertures.

As shown in the figures, the diffraction patterns are similar to each other. The number and the distance between orders match in both cases. Some effects visualized in the simulation are not observable in the experimental image and vice-versa, mainly because it is difficult to predict the effects produced by the gaps between micromirrors and other structures present in the DMD and it is also difficult to correctly adjust the brightness of the simulation and the brightness of the experiment, without saturating parts of the image and with a correct sampling.

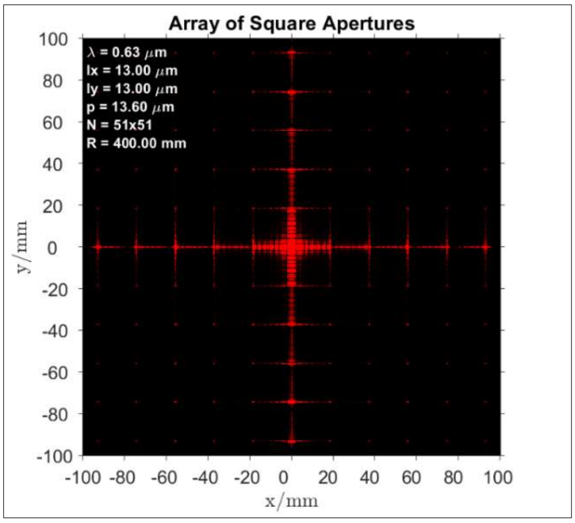

Figure 14. Diffraction pattern simulation of a two-dimensional array of square apertures, for a coherent light source, with a wavelength of 632 nm, passing through an array of 51x51 square apertures, with 13 µm in size and with a spatial frequency of 13.6 µm, projected onto a target at 400 mm distance with 200x200 mm area.

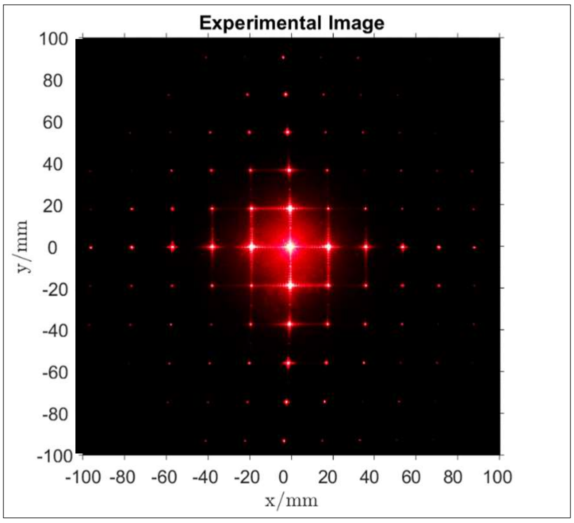

Figure 15. Experimental image taken in the laboratory, for a Melles Griot Helium-Neon Laser, with a wavelength of 632.8 nm, falling in a DMD array of square micromirrors in the FLAT state, with 13 µm in size and with a spatial frequency of 13.6 µm, projected onto a target at a focal distance of 400 mm.

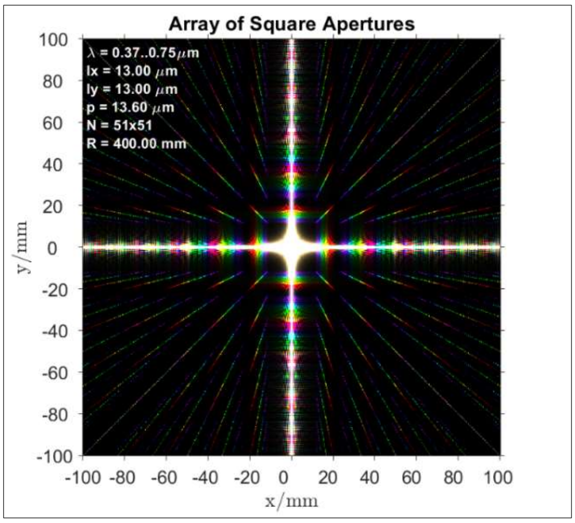

Figure 16. Diffraction pattern simulation of a two-dimensional array of square apertures, for a black body at a temperature of 10 000 K, with a wavelength range from 375 nm to 750 nm, passing through an array of 51x51 square apertures, with 13 µm in size and with a spatial frequency of 13.6 µm, projected onto a target at 400 mm distance with 200x200 mm area.

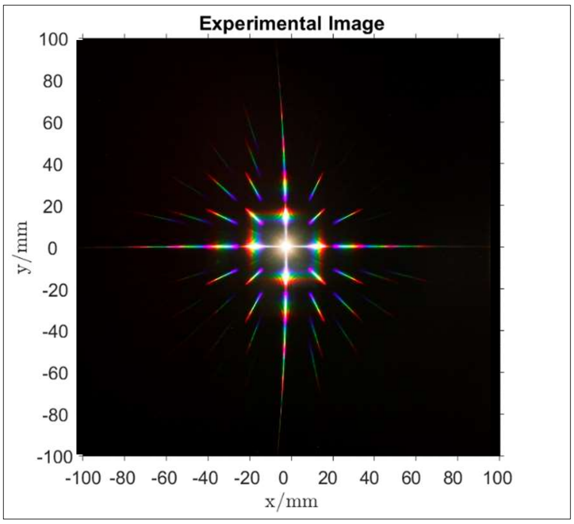

Figure 17. Experimental image taken in the laboratory, for a Thorlabs OSL1-EC Fiber Light Source, with a black body equivalent temperature of 3200 K, falling in a DMD array of square micromirrors in the FLAT state, with 13 µm in size and with a spatial frequency of 13.6 µm, projected onto a target at a focal distance of 400 mm.

Figures 18 (simulation) and 19 (experimental image) shows the diffraction patterns observable with a coherent light source, with a wavelength of 632 nm, for a two-dimensional array of tilted micromirrors. Figures 20 (simulation) and 21 (experimental image) shows the diffraction patterns observable with an incoherent light source, with a black body equivalent temperature of 3200 K, for a two-dimensional array of tilted micromirrors.

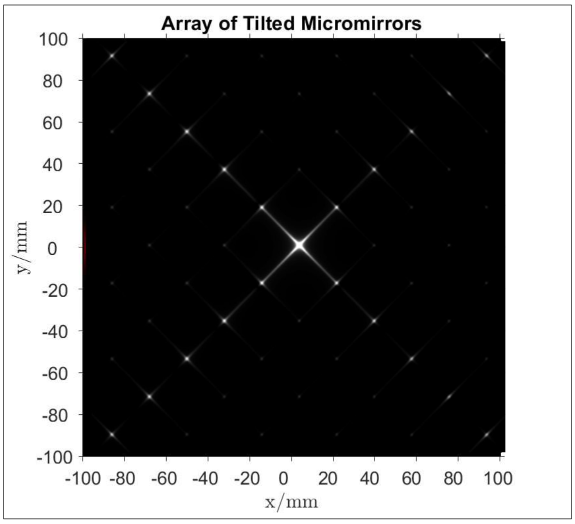

Figure 18. Diffraction pattern simulation of a two-dimensional array of tilted micromirrors, for a coherent light source, with a wavelength of 632 nm, falling in an array of 51x51 micromirrors rotated 12°, with 13 µm in size and with a spatial frequency of 13.6 µm, projected onto a target at 400 mm distance with 200x200 mm area.

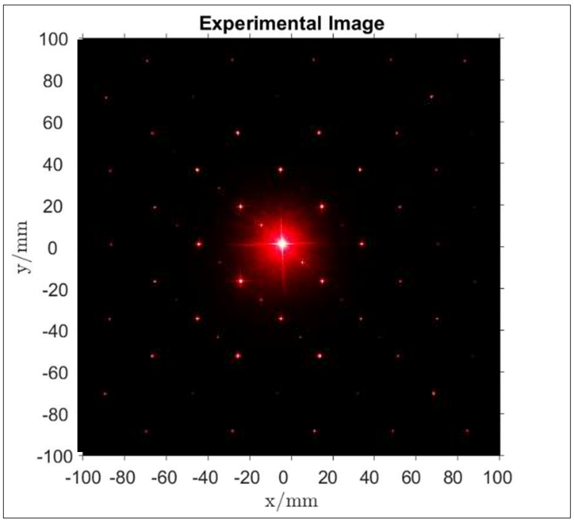

Figure 19. Experimental image taken in the laboratory, for a Melles Griot Helium-Neon Laser, with a wavelength of 632.8 nm, falling in a DMD array of micromirrors rotated 12°, with 13 µm in size and with a spatial frequency of 13.6 µm, projected onto a target at a focal distance of 400 mm.

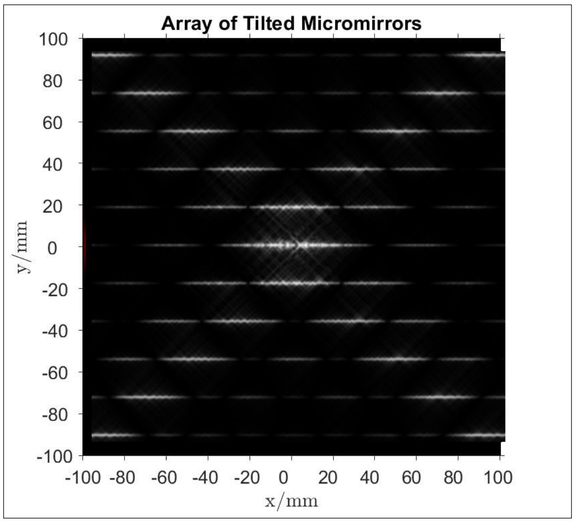

Figure 20. Diffraction pattern simulation of a two- dimensional array of tilted micromirrors, for a black body at a temperature of 10 000 K, with a wavelength range from 375 nm to 750 nm, falling in an array of 51x51 micromirrors rotated 12°, with 13 µm in size and with a spatial frequency of 13.6 µm, projected onto a target at 400 mm distance with 200x200 mm area.

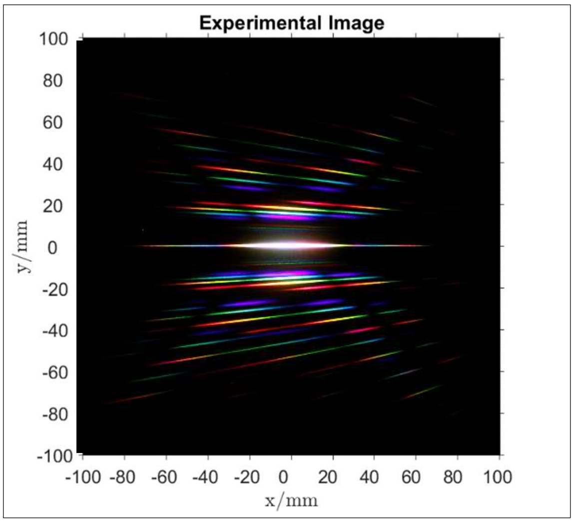

Figure 21. Experimental image taken in the laboratory, for a Thorlabs OSL1-EC Fiber Light Source, with a black body equivalent temperature of 3200 K, falling in a DMD array of micromirrors rotated 12°, with 13 µm in size and with a spatial frequency of 13.6 µm, projected onto a target at a focal distance of 400 mm.

4. Conclusions

From simulations and experimental activities, we concluded that the DMD, in one of the ON or OFF operational states, acts as a blazed grating [1], commonly used in some spectrographs. The dispersion of light with the increase of wavelength range needs to be taken into account, when a DMD is chosen to be implemented in a specific application.

For a coherent light source, it is possible to efficiently collect light from the main order expressed in the diffraction pattern, however, using a white source, the orders are not point-like. In this case, it will be difficult to efficiently couple light from the Fourier plane without losing part of the radiation and part of the spectrum, expressed as a stripped pattern in the diffraction pattern.

The next steps in this work are to finish the development of the code used to simulate the different diffraction patterns and the development of a methodology to collect light after reflection from the DMD, emitted from an incoherent white source, minimizing the loss of light and the loss of the spectral component.

5. Acknowledgments

This work is financed by Portuguese national funds through FCT - Fundação para a Ciência e a Tecnologia, I.P. in the scope of the research grants: PD/BD/150443/2019, UIDB/04434/2020 & UIDP/04434/2020.

References

[1] Dudley D, Duncan WM and Slaughter J 2003 Emerging digital micromirror device (DMD) applications *Proc. SPIE 4985* MOEMS Display and Imaging Systems
[2] Lee B 2018 Introduction to ±12 degree orthogonal digital micromirror devices (DMDs) *TI Application Report DLPA008B*
[3] Markandey V, Clatanoff T and Pettitt G 1996 Video processing for DLP display systems *Proc. SPIE 2666* Image and Video Processing IV
[4] Texas Instruments – Applications & designs https://www.ti.com/applications/overview.html (accessed: 23 May 2022)
[5] Robberto M, Cimatti A, Jacobsen A, Zamkotsian F and Zerbi F 2009 Applications of DMDs for astrophysical research *Proc. SPIE 7210*, Emerging Digital Micromirror Device Based Systems and Applications
[6] MacKenty J, Greenhouse M, Green R, Sparr L, IV R Ohl and Winsor R 2003 IRMOS: an infrared multi-object spectrometer using a MEMs micromirror array *Proc. SPIE 4841*, Instrument Design and Performance for Optical/Infrared Ground-based Telescopes
[7] Meyer R, Kearney K, Ninkov Z, Cotton C, Hammond P and Statt B, 2004 RITMOS: a micromirror-based multi-object spectrometer *Proc. SPIE 5492*, Ground-based Instrumentation for Astronomy
[8] Zamkotsian F, Spano P, Lanzoni P, Ramarijaona H, Moschetti M, Riva M, Bon W, Nicastro L, Molinari E, Cosentino R et al. 2014 BATMAN: a DMD-based multi-object spectrograph on Galileo telescope *Proc. SPIE 9147* Ground-based and Airborne Instrumentation for Astronomy V
[9] Zamkotsian F, Grassi E, Lanzoni P, Barette R, Fabron C, Tangen K, Marchand L and Duvet L, 2010 DMD chip space evaluation for ESA's EUCLID mission *Proc. SPIE 7596* Emerging Digital Micromirror Device Based Systems and Applications II
[10] Ayoub A and Psaltis D, 2021 High speed, complex wavefront shaping using the digital micro-mirror device *Sci Rep 11*, 18837
[11] Texas Instruments – DLP7000 https://www.ti.com/product/DLP7000 (accessed: 08 February 2022).
[12] Goodman J 2002 *Introduction to Fourier Optics 2nd edition* McGraw-Hill New York USA
[13] Texas Instruments – DLP7000 DLP 0.7 XGA 2x LVDS Type A DMD Datasheet https://www.ti.com/lit/ds/symlink/dlp7000.pdf (accessed: 04 April 2022).